Supporting Information

Tuning radical interactions in trisradical tricationic complexes by varying host cavity sizes

Kang Cai, Yi Shi, Changsu Cao, Suneal Vemuri, Binbin Cui, Dengke Shen, Huang Wu, Long Zhang, Yunyan Qiu, Hongliang Chen, Yang Jiao, Charlotte L. Stern, Fehaid M. Alsubaie, Hai Xiao, Jun Li and J. Fraser Stoddart**

Table of Contents

Section A. General Methods

All reagents were purchased from commercial suppliers and used without further purification. Compounds 2,5-bis(bromomethyl)thiophene[S1], **HS**•$2PF_6$[S2], cyclobis(paraquat-*p*-phenylene) tetrakis(hexafluorophosphate)[S3] (**BB**•$4PF_6$) were prepared according to literature procedures. Thin layer chromatography (TLC) was performed on silica gel 60 F254 (E. Merck). Column chromatography was carried out on silica gel 60F (Merck 9385, 0.040–0.063 mm). UV/Vis Spectra were recorded at room temperature on a Shimadzu UV-3600 spectrophotometer. Nuclear magnetic resonance (NMR) spectra were recorded on Agilent DD2 500 with working frequencies of 500 MHz for ^{1}H and 125 MHz for ^{13}C nuclei. Chemical shifts were reported in ppm relative to the signals corresponding to the residual non-deuterated solvents (CD_3CN: δ_H =1.94 ppm and δ_C = 118.26 ppm for ^{13}CN). High-resolution mass spectra (HR-ESI) were measured on a Finnigan LCQ iontrap mass spectrometer. Electron paramagnetic resonance (EPR) measurements at X-band (9.5 GHz) were performed with a Bruker Elexsys E580, equipped with a variable Q dielectric resonator (ER-4118X-MD5-W1). All samples were prepared in an Ar-filled atmosphere. Samples were loaded into quartz 1.4 mm tubes and sealed with a clear ridged UV doming epoxy (IllumaBond 60-7160RCL) and used immediately after preparation. Cyclic voltammetry (CV) were carried out at room temperature in Ar-purged MeCN solutions with a Gamry Multipurpose instrument (Reference 600) interfaced to a PC. CV Experiments were performed using a glassy carbon working electrode (0.071 cm^2). The electrode surface was polished routinely with 0.05 μm alumina-water slurry on a felt surface immediately before use. The counter electrode was a Pt coil and the reference electrode was Ag/AgCl electrode. The concentration of the supporting electrolyte tetrabutylammonium hexafluorophosphate (NBu_4PF_6) was 0.1 M.

Section B. Synthetic Protocols

General Procedure for TBAI catalyzed cyclization:

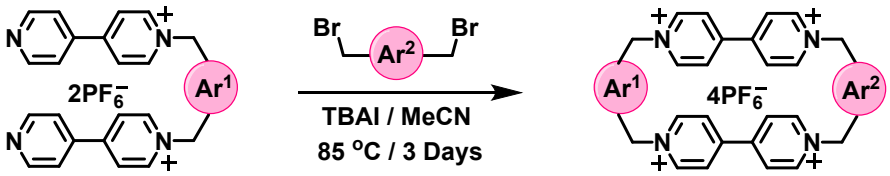

HS•2PF$_6$ **Box•4PF$_6$**

HS•2PF_6 (1 mmol), **Ar-2Br** (1 mmol) and TBAI (20% mmol) in dry MeCN (500 mL) was stirred at 85 °C for 5 days. Then the solution was cooled down to room temperature and TBACl was added to precipitate the crude product from the MeCN solution. The precipitate was collected by filtration and washed with MeCN for three times. The precipitate was then dissolved in H_2O, reprecipitated as PF_6^- salt (white) by adding solid NH_4PF_6 (~5% (w/v)), and collected by filtration. This crude material was subjected to column chromatography using silica gel and 2% NH_4PF_6 in Me_2CO (w/v) as the eluents. The products were collected, and the solvents were removed *in vacuo*. The white solid was washed with H_2O, yielding pure **Box**·4PF_6. The syntheses of **mpBB**•4PF_6[S4] and **pyBB**•4PF_6[S4] has been reported in previous literature.

mpBB•4PF_6: Yield: 46%. mp>270 °C (decomposed). ^{1}H NMR (500 MHz, CD_3CN, 298 K) δ 9.01 (d, *J* = 6.7 Hz, 4H), 8.87 (d, *J* = 6.7 Hz, 4H), 8.10 (d, *J* = 6.7 Hz, 4H), 8.07 (d, *J* = 6.7 Hz, 4H), 7.80 (d, *J* = 7.8 Hz, 2H), 7.65 (s, 5H), 5.82 (s, 4H), 5.80 (s, 4H). ^{13}C NMR (125 MHz, CD_3CN, 298 K) δ 207.4, 151.0, 150.8, 146.2, 145.8, 137.5, 135.3, 133.1, 131.9, 131.3, 130.3, 128.4, 128.1, 118.3, 65.9, 65.2, 30.8.

pyBB•4PF_6: Yield: 52%. mp>270 °C (decomposed). ^{1}H NMR (500 MHz, CD_3CN) δ 8.98 (d, *J* = 6.6 Hz, 4H), 8.83 (d, *J* = 6.6 Hz, 4H), 8.08 (d, *J* = 6.8 Hz, 4H), 8.06-8.03 (m, 5H), 7.76 (d, *J* = 7.5 Hz, 2H), 7.63 (s, 4H), 5.79 (s, 4H), 5.77 (s, 4H). ^{13}C NMR (126 MHz, CD_3CN) δ 207.4, 152.9, 151.2, 151.1, 146.8, 145.6, 141.2, 137.8, 131.3, 128.6, 127.8, 126.5, 66.1, 65.9, 30.8.

DThBB•4PF_6: Yield: 30%. mp>270 °C (decomposed). ^{1}H NMR (500 MHz, CD_3CN, 298 K) δ 8.82 (d, *J* = 6.9 Hz, 8H), 8.18 (d, *J* = 6.9 Hz, 8H), 7.48 (s, 4H), 6.00 (s, 4H). ^{13}C NMR (125 MHz,

CD_3CN, 298 K) δ 207.4, 151.0, 146.2, 141.0, 132.4, 128.4, 60.7, 30.9. HR-ESI MS: Calcd for $C_{32}H_{28}F_{24}N_4P_4S_2$: m/z = 967.0675 $[M - PF_6^-]^+$; found: 967.0678.

ThBB•4PF_6: Yield: 42%. mp>270 °C (decomposed). ^{1}H NMR (500 MHz, CD_3CN, 298 K) δ 8.90 (d, J = 6.5 Hz, 4H), 8.83 (d, J = 6.7 Hz, 4H), 8.18 (d, J = 6.2 Hz, 8H), 7.61 (s, 4H) 7.47 (s, 2H), 5.98 (s, 4H), 5.80 (s, 4H). ^{13}C NMR (125 MHz, CD_3CN, 298 K) δ 150.7, 146.2, 146.1, 140.5, 137.3, 132.5, 131.4, 128.4, 128.2, 65.8, 60.5. HR-ESI MS: Calcd for $C_{34}H_{30}F_{24}N_4P_4S$: m/z = 961.1111 $[M - PF_6^-]^+$; found: 961.1112.

Section C. ^{1}H NMR Spectroscopy

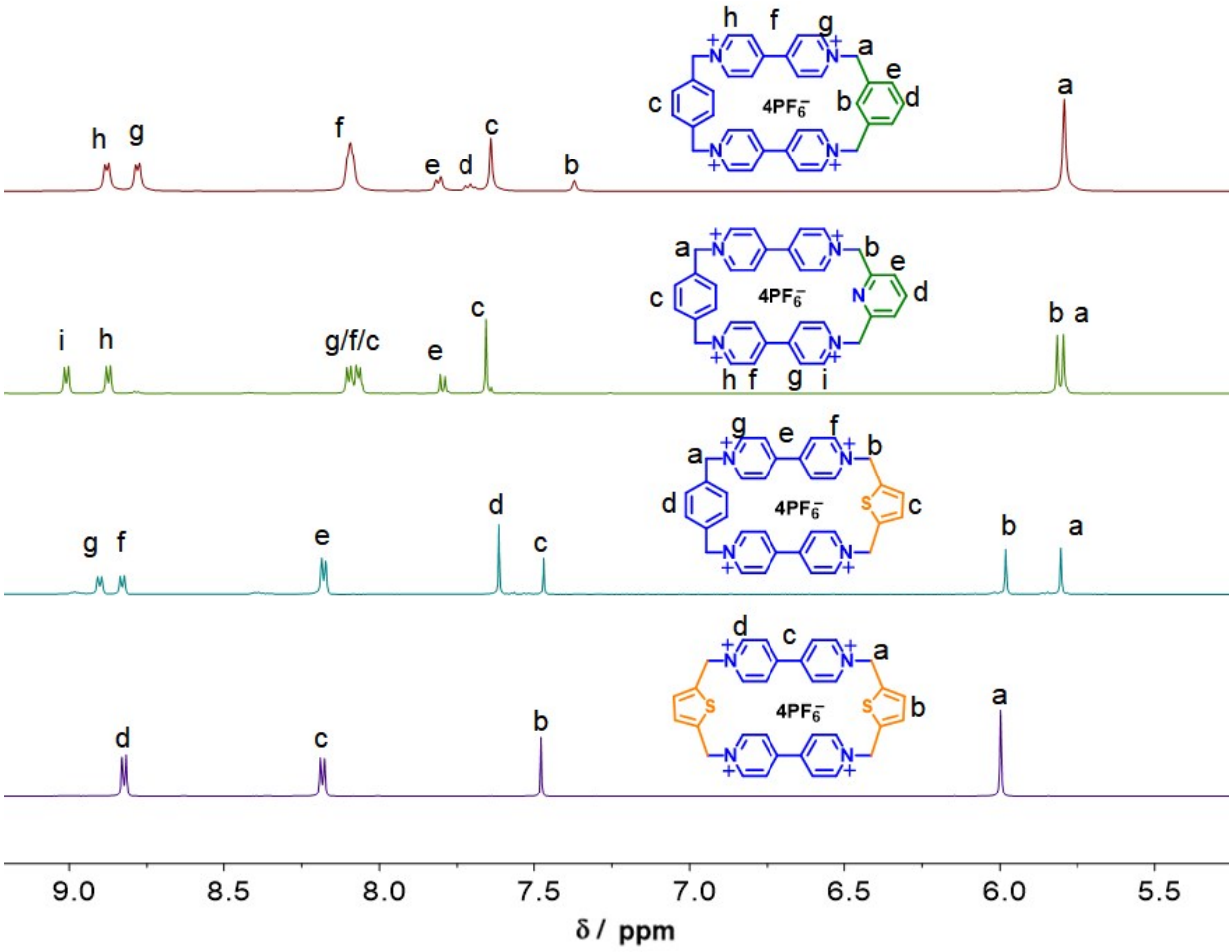

Figure S1. Stacked ^{1}H NMR spectra (500 MHz, CD_3CN, 298 K) of **mpBB**•4PF_6, **pyBB**•4PF_6, **ThBB**•4PF_6 and **DThBB**•4PF_6

Section D. UV-Vis-NIR Titration

Stock solutions of the fully oxidized viologen derivatives **MV•** $2PF_6$, **mpBB•** $4PF_6$, **pyBB•** $4PF_6$, **ThBB•**$4PF_6$ and **DThBB•**$4PF_6$ were prepared in an N_2 glovebox. The stock solutions were reduced over actviated Zn dust for 10 to15 min with stirring and then filtered to provide deep blue solutions.

Syringes were employed to measure and dilute the radical stock solutions to the desired to measure and dilute the radical stock solutions to the desired concentrations prior to measurements. Measurements of the association constants (K_a) for the formation of trisradical complexes between the $\mathbf{MV}^{\bullet+}$ radical cation and different diradical dicationic cyclophanes in MeCN were carried out under N_2 in a glovebox. The titration procedure is same as the previously[S6] reported protocols.

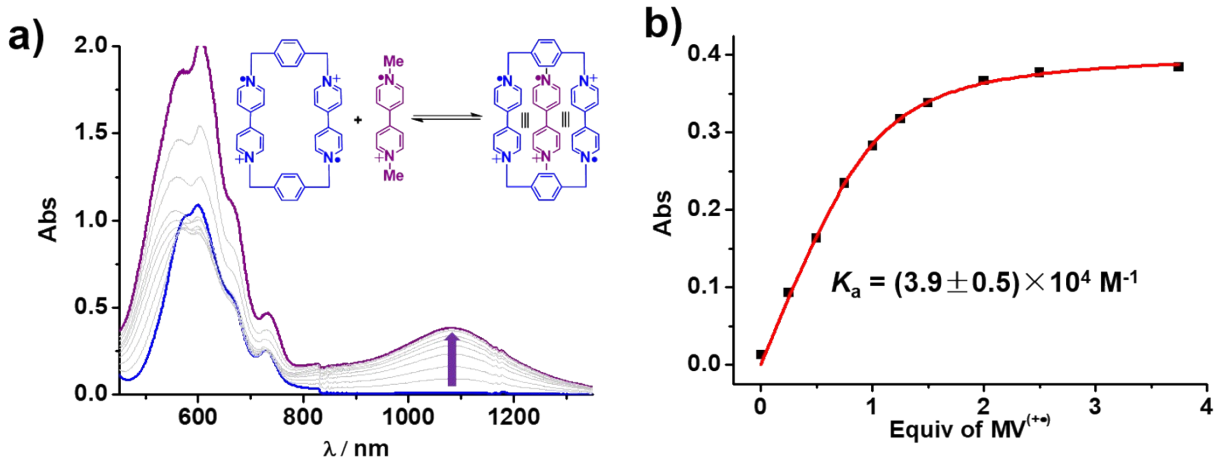

Figure S2. a) Stacked UV-Vis-NIR spectra obtained by titrating $\mathbf{MV}^{\bullet+}$ into a solution of $\mathbf{BB}^{2(\bullet+)}$ (0.25 mM in MeCN); b) Binding isotherm simulation. Optical length: 2 mm.

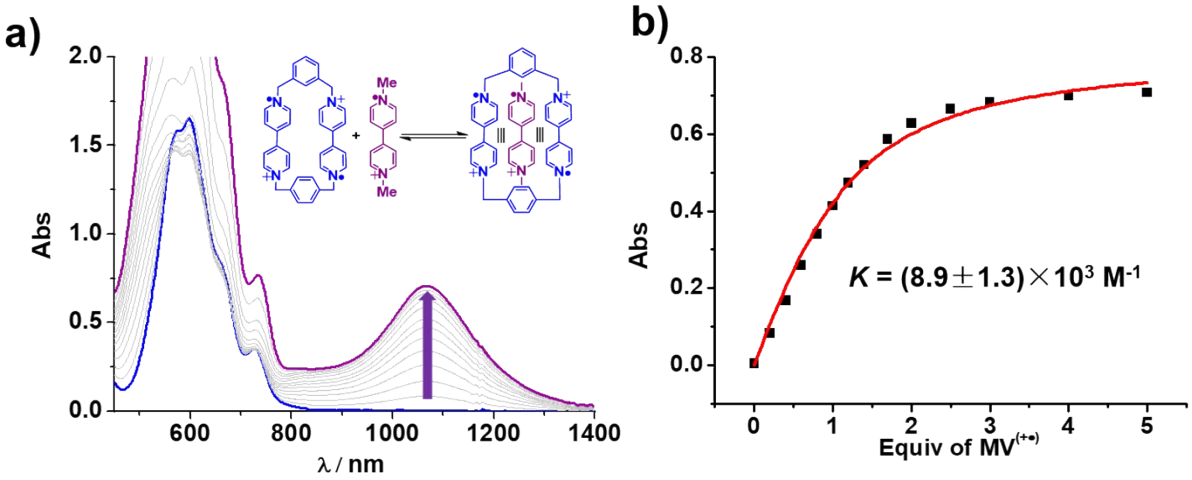

Figure S3. a) Stacked UV-Vis-NIR spectra obtained by titrating **MV**$^{\bullet+}$ into a solution of **mpBB**$^{2(\bullet+)}$ (0.25 mM in MeCN); b) Binding isotherm simulation. Optical length: 2 mm.

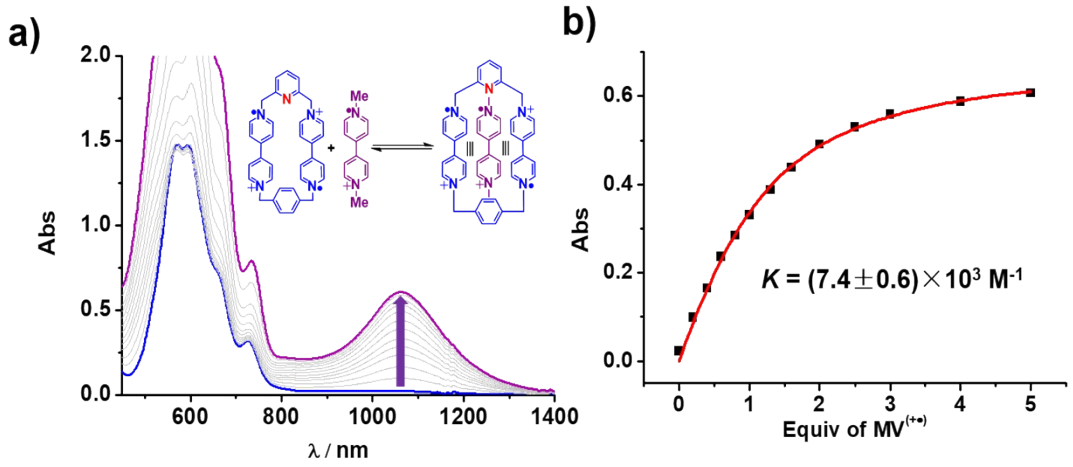

Figure S4. a) Stacked UV-Vis-NIR spectra obtained by titrating **MV**$^{\bullet+}$ into a solution of **pyBB**$^{2(\bullet+)}$ (0.25 mM in MeCN); b) Binding isotherm simulation. Optical length: 2 mm.

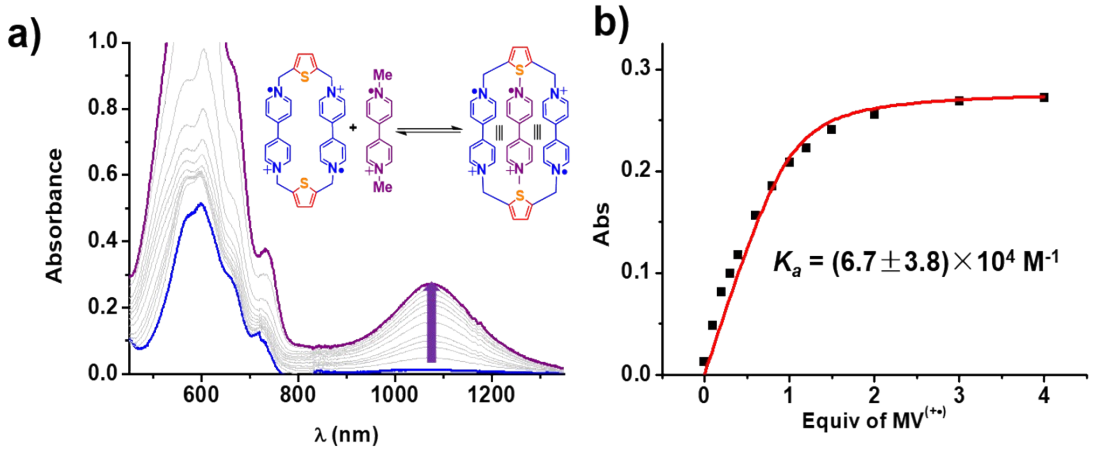

Figure S5. a) Stacked UV-Vis-NIR spectra obtained by titrating **MV**$^{\bullet+}$ into a solution of **DThBB**$^{2(\bullet+)}$(0.20 mM in MeCN); b) Binding isotherm simulation. Optical length: 2 mm.

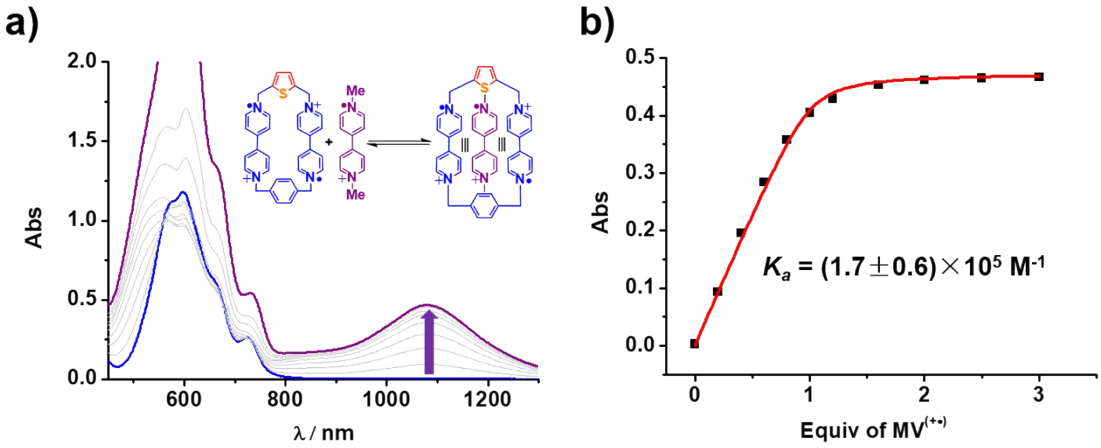

Figure S6. a) Stacked UV-Vis-NIR spectra obtained by titrating $\mathbf{MV}^{\bullet+}$ into a solution of $\mathbf{ThBB}^{2(\bullet+)}$ (0.25 mM in MeCN); b) Binding isotherm simulation. Optical length: 2mm.

Section E. Electrochemistry

General Procedures for CV Experiments: Samples for cyclic voltammetry (CV) were prepared using an electrolyte solution of 0.1 M $[Bu_4N][PF_6]$ in MeCN that was sparged with Ar to remove O_2. The CVs presented in the main text of the manuscript and herein were recorded under Ar using a glassy carbon working electrode, a Pt wire or Pt mesh counter electrode, a silver wire quasi-reference electrode, and an internal standard of ferrocene.

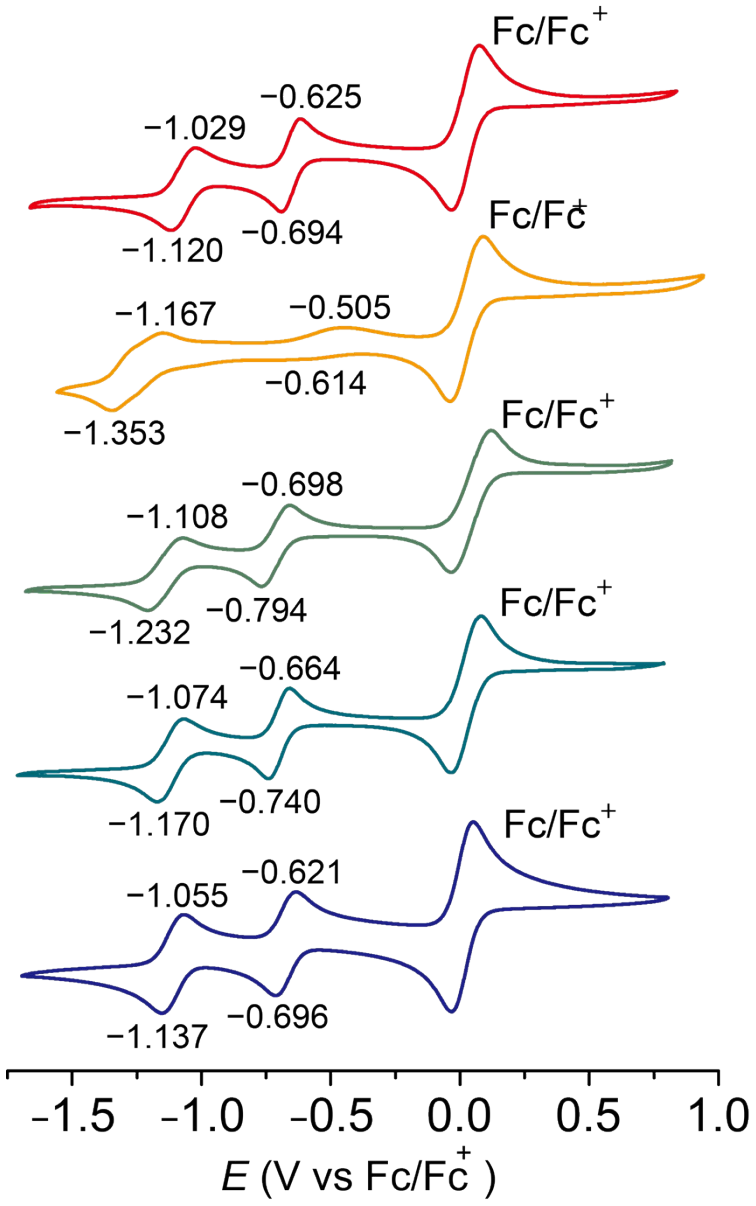

Figure S7. Cyclic voltammograms of a) **DThBB**·4PF$_6$; b) **ThBB**·4PF$_6$; c) **mpBB**·4PF$_6$; d) **PyBB**·4PF$_6$; e) BB·4PF$_6$

Section F. Crystallographic Characterization

The crystal structure of **DThBB•**4PF has been reported in previous[S1] literature. All crystallographic data are available free of charge from the Cambridge Crystallographic Data Centre via www.ccdc.cam.ac.uk/data_request/cif. The CCDC numbers are from 1955702 to 1955711.

1) mpBB•4PF$_6$

a) Methods. Single crystals of **mpBB**•4PF$_6$ were grown by slow vapor diffusion of $^{i}Pr_2O$ into the 1.0 mM MeCN solution of **mpBB**•4PF$_6$ during a 4-day period.

b) Crystal Data. Monoclinic, space group $P2_1/c$ (no. 14), a = 7.4563(11), b = 20.125(3), c = 13.948(2) Å, β = 91.831(8)°, V = 2092.0(5) Å^3, Z = 2, T = 99.99 K, μ(CuK$_\alpha$) = 3.004 mm^{-1}, *Dcalc* = 1.747 g/mm^3, 12508 reflections measured (7.714 ≤ 2Θ ≤ 130.148), 3544 unique (R_{int} = 0.0346, R_{sigma} = 0.0371) which were used in all calculations. The final R_1 was 0.0485 ($I > 2\sigma(I)$) and wR_2 was 0.1248 (all data).

c) Refinement Details. Rigid bond restraints were imposed on the displacement parameters as well as restraints on similar amplitudes separated by less than 1.7 Å.

d) Solvent Treatment Details. The solvent masking procedure as implemented in Olex2 was used to remove the electronic contribution of solvent molecules from the refinement. As the exact solvent content is not known, only the atoms used in the refinement model are reported in the formula here. Total solvent accessible volume / cell = 348.6 Å^3 [14.5%] Total electron count / cell = 80.0.

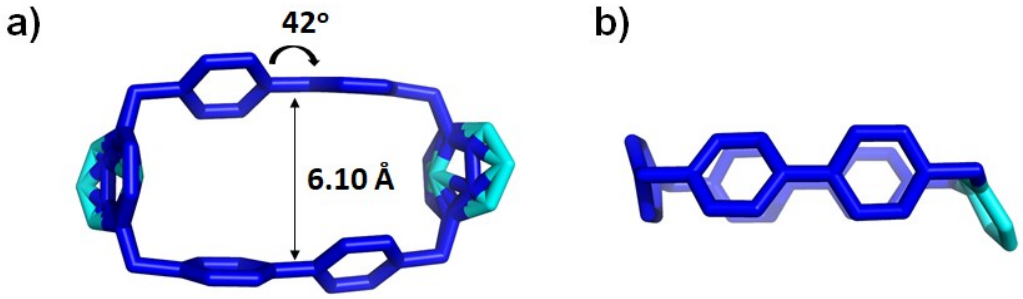

Figure S8. Side view (a) and top view (b) of solid-state structure of **mpBB**•4PF$_6$. Solvent molecules and counterions are omitted for the sake of clarity.

2) pyBB•4PF$_6$

a) Methods. Single crystals of **pyBB**•4PF$_6$ were grown by slow vapor diffusion of $^{i}Pr_2O$ into the 1.0 mM MeCN solution of **pyBB**•4PF$_6$ during a 4-day period.

b) Crystal Data. Triclinic, space group *P-1* (no. 2), a = 11.2904(11), b = 16.9439(18), c = 24.966(3) Å, α = 75.157(10), β = 86.061(11), γ = 86.580(9)°, V = 4601.5(8) Å^3, Z = 4, T = 99.98 K, μ(CuK$_\alpha$) = 2.739 mm^{-1}, D_{calc} = 1.590 g/mm^3, 34289 reflections measured (3.666 ≤ 2Θ ≤ 120), 13418 unique (R_{int} = 0.1817, R_{sigma} = 0.1636) which were used in all calculations. The final R_1 was 0.2375 ($I > 2\sigma(I)$) and wR_2 was 0.6050 (all data).

c) Refinement Details. The enhanced rigid-bond restraint (SHELX keyword RIGU) was applied globally[S2]. Distance restraints were imposed on the PF_6^- anions.

d) Solvent Treatment Details. The solvent masking procedure as implemented in Olex2 was used to remove the electronic contribution of solvent molecules from the refinement. As the exact solvent content is not known, only the atoms used in the refinement model are reported in the formula here. Total solvent accessible volume / cell = 319.1 Å^3 [6.9%] Total electron count / cell = 117.5

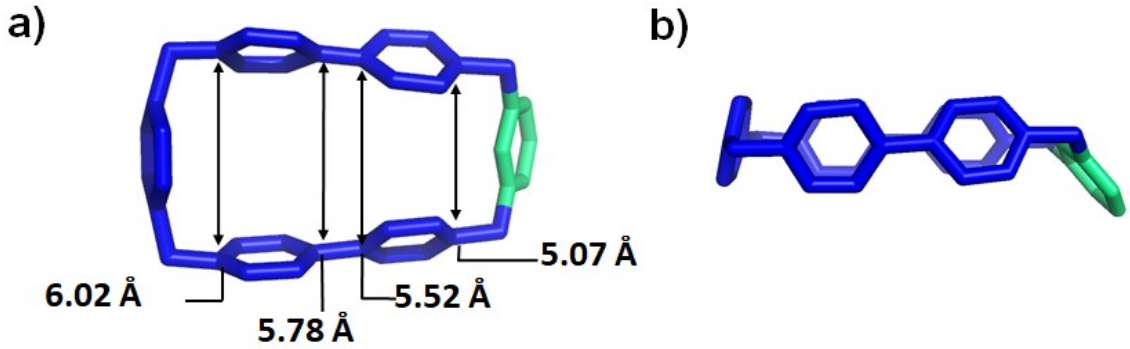

Figure S9. Side view (a) and top view (b) of solid-state structure of **pyBB**•4PF$_6$. Solvent molecules and counterions are omitted for the sake of clarity.

3) ThBB•4PF$_6$

a) Methods. Single crystals of **ThBB**•4PF$_6$ were grown by slow vapor diffusion of ^{i}Pr$_2$O into the 1.0 mM MeCN solution of **ThBB**•4PF$_6$ during a 5-day period.

b) Crystal Data. Triclinic, space group $P\bar{1}$ (no. 2), a = 13.6030(13), b = 13.8062(13), c = 16.0216(16) Å, α = 101.314(6)°, β = 111.832(6)°, γ = 107.987(6)°, V = 2486.3(4) Å^3, Z = 4, T = 100.02 K, μ(MoK$_\alpha$) = 0.317 mm^{-1}, D_{calc} = 1.533 g/mm^3, 33847 reflections measured (2.926 ≤ 2Θ ≤ 53.042), 10194 unique (R_{int} = 0.0787, R_{sigma} = 0.1146) which were used in all calculations. The final R_1 was 0.1355 ($I > 2\sigma(I)$) and wR_2 was 0.4408 (all data).

c) Refinement Details. Distance restraints were imposed on the disordered PF_6^- anions and disordered rings. Rigid bond restraints were imposed on the displacement parameters as well as restraints on similar amplitudes separated by less than 1.7 Å on the disordered atoms.

d) Solvent Treatment Details. The solvent masking procedure as implemented in Olex2 was used to remove the electronic contribution of solvent molecules from the refinement. As the exact solvent content is not known, only the atoms used in the refinement model are reported in the formula here. Total solvent accessible volume / cell = 348.6 Å^3 [14.5%] Total electron count / cell = 80.0.

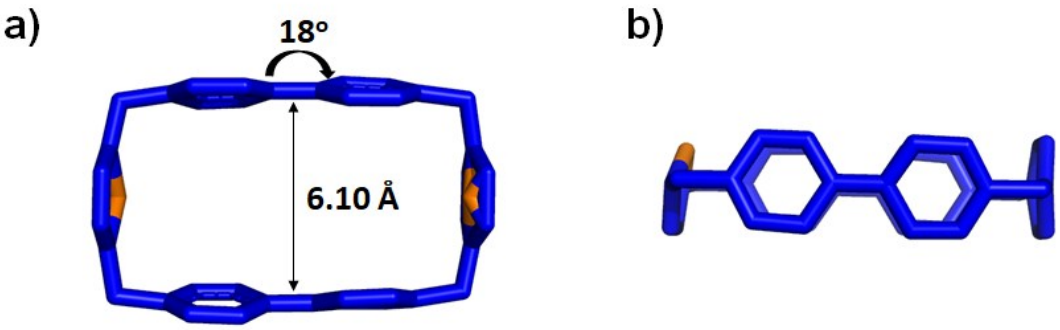

Figure S10. Side view (a) and top view (b) of solid-state structure of **ThBB**•4PF$_6$. Solvent molecules and counterions are omitted for the sake of clarity.

4) mpBB•2PF$_6$

a) Methods. Single crystals of **mpBB**•2PF$_6$ were grown in a glovebox under Ar by preparing a 2 mL solution of 1.0 mM **mpBB**•4PF$_6$ in MeCN, followed by the addition of an excess of Zn dust.

The resulting suspension was filtered and the filtrate divided between eight culture tubes. Slow vapor diffusion of $^{i}Pr_2O$ into the MeCN solutions led to the formation of purple single single crystals during a 5-day period.

b) Crystal data. Orthorhombic, space group *Cmc21* (no. 36), a = 19.886(4), b = 20.698(4), c = 20.515(4) Å, V = 8444(3) Å^3, Z = 4, T = 100.01 K, $\mu(CuK_\alpha)$ = 2.051 mm^{-1}, D_{calc} = 1.486 g/mm^3, 31740 reflections measured (6.164 ≤ 2Θ ≤ 133.056), 7349 unique (R_{int} = 0.0421, R_{sigma} = 0.0458) which were used in all calculations. The final R_1 was 0.0542 ($I > 2\sigma(I)$) and wR_2 was 0.1579 (all data).

c) Refinement details. The enhanced rigid-bond restraint was applied on the disordered PF_6^- anions. Distance restraints were also imposed on the disordered anions.

d) Solvent Treatment Details. The solvent masking procedure as implemented in Olex2 was used to remove the electronic contribution of solvent molecules from the refinement. As the exact solvent content is not known, only the atoms used in the refinement model are reported in the formula here. Total solvent accessible volume / cell = 366.3 Å^3 [4.3%] Total electron count / cell = 107.8

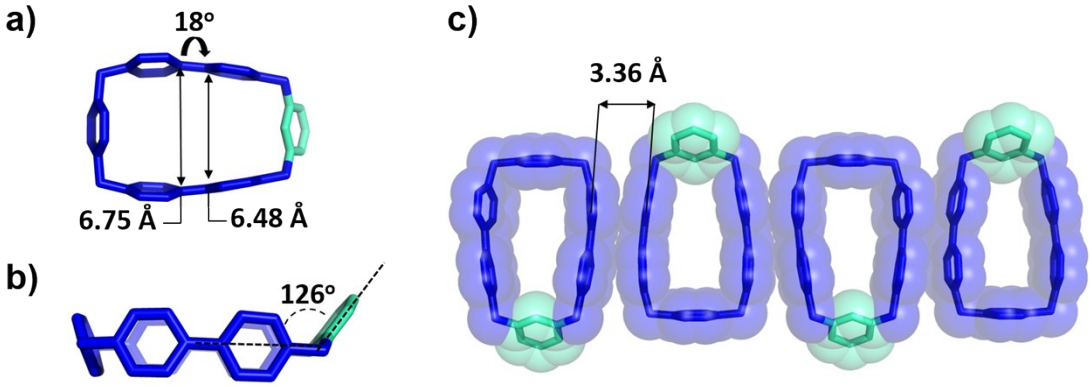

Figure S11. Solid-state (super)structure of **mpBB**•2PF_6. a) Side view, b) top view, c) 1D packing along *c*-axis. Solvent molecules and counterions are omitted for the sake of clarity.

5) DThBB•2PF$_6$

a) Methods. Single crystals of **DThBB**•2PF_6 were grown in a glovebox under Ar by preparing a 2 mL solution of 1.0 mM **DThBB**•4PF_6 in MeCN, followed by the addition of an excess of Zn dust.

The resulting suspension was filtered and the filtrate divided between eight culture tubes. Slow vapor diffusion of $^{i}Pr_2O$ into the MeCN solutions led to the formation of purple single crystals during a 5-day period.

b) Crystal data. Orthorhombic, space group *Pbam* (no. 55), a = 10.3821(5), b = 21.5348(9), c = 9.6558(4) Å, V = 2158.81(16) Å^3, Z = 2, T = 99.98 K, μ(CuK$_\alpha$) = 2.526 mm^{-1}, D_{calc} = 1.266 g/mm^3, 12125 reflections measured (8.212 ≤ 2Θ ≤ 131.928), 1999 unique (R_{int} = 0.0327, R_{sigma} = 0.0244) which were used in all calculations. The final R_1 was 0.0471 ($I > 2\sigma(I)$) and wR_2 was 0.1561 (all data).

c) Refinement details. No special refinement necessary.

d) Solvent treatment details. The solvent masking procedure as implemented in Olex2 was used to remove the electronic contribution of solvent molecules from the refinement. As the exact solvent content is not known, only the atoms used in the refinement model are reported in the formula here. Total solvent accessible volume / cell = 646.5 Å^3 [29.9%] Total electron count / cell = 149.4.

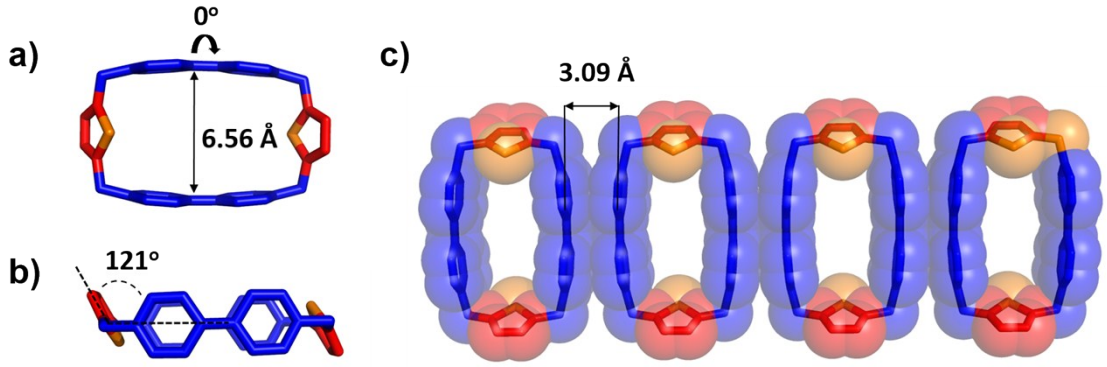

Figure S12. Solid-state (super)structure of **DThBB**•2PF$_6$. a) Side view, b) top view, c) 1D packing along *c*-axis. Solvent molecules and counterions are omitted for the sake of clarity.

6) ThBB•2PF$_6$

a) Methods. Single crystals of **ThBB**•2PF$_6$ were grown in a glovebox under Ar by preparing a 2 mL solution of 1.0 mM **ThBB**•4PF$_6$ in MeCN, followed by the addition of an excess of Zn dust. The resulting suspension was filtered and the filtrate divided between eight culture tubes. Slow

vapor diffusion of $^{i}Pr_2O$ into the MeCN solutions led to the formation of purple single crystals during a 5-day period.

b) Crystal data. Orthorhombic, space group *Pbam* (no. 55), a = 10.2660(6), b = 21.7433(14), c = 9.8244(6) Å, V = 2193.0(2) Å^3, Z = 2, T = 100.01 K, μ(CuKα) = 2.050 mm^{-1}, D_{calc} = 1.237 g/mm^3, 11620 reflections measured (8.132 ≤ 2Θ ≤ 128.764), 1953 unique (R_{int} = 0.0463, R_{sigma} = 0.0299) which were used in all calculations. The final R_1 was 0.0509 ($I > 2\sigma(I)$) and wR_2 was 0.1601 (all data).

c) Refinement details. The enhanced rigid-bond restraint (SHELX keyword RIGU) was applied on the disordered sulfur atom.

d) Solvent treatment details. The solvent masking procedure as implemented in Olex2 was used to remove the electronic contribution of solvent molecules from the refinement. As the exact solvent content is not known, only the atoms used in the refinement model are reported in the formula here. Total solvent accessible volume / cell = 625.1 Å^3 [28.5%] Total electron count / cell = 157.8.

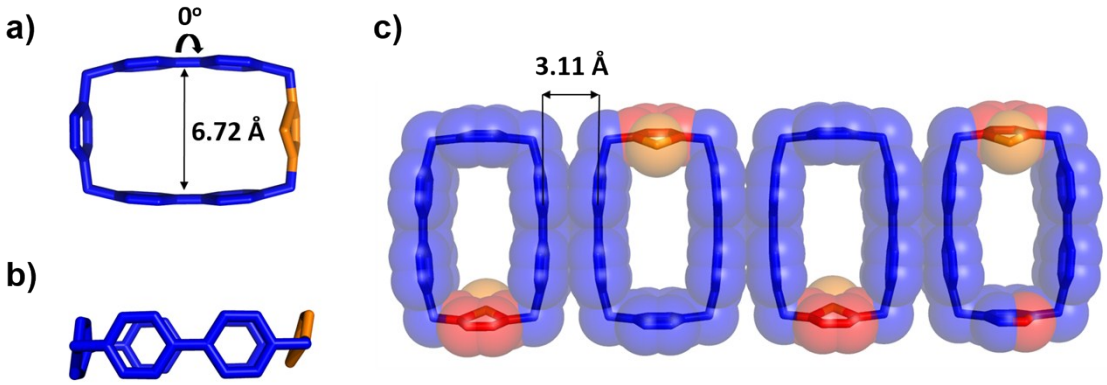

Figure S13. Solid-state (super)structure of **ThBB**•2PF$_6$. a) Side view, b) top view, c) 1D packing along *c*-axis. Solvent molecules and counterions are omitted for the sake of clarity.

7) MV⊂mpBB•3PF$_6$

a) Methods. Single crystals of **MV⊂mpBB**•3PF$_6$ were grown in a glovebox under Ar by preparing a 2 mL solution of 1.0 mM **mpBB**•4PF$_6$ and 1.0 mM **MV**•2PF$_6$ in MeCN, followed by the addition

of an excess of Zn dust. The resulting suspension was filtered and the filtrate divided between eight culture tubes. Slow vapor diffusion of $^{i}Pr_2O$ into the MeCN solutions led to the formation of purple single crystals during a 5-day period.

b) Crystal data. Orthorhombic, space group *Pbam* (no. 55), a = 14.1423(6), b = 21.9108(7), c = 9.5937(3) Å, V = 2972.79(18) Å^3, Z = 2, T = 100(2) K, $\mu(CuK_\alpha)$ = 1.748 mm^{-1}, D_{calc} = 1.276 g/mm^3, 14176 reflections measured ($7.44 \leq 2\Theta \leq 130.122$), 2679 unique ($R_{int} = 0.0455$, $R_{sigma} = 0.0360$) which were used in all calculations. The final R_1 was 0.1009 ($I > 2\sigma(I)$) and wR_2 was 0.3523 (all data).

c) Refinement Details. Distance restraints were imposed on the disordered atoms as well as a "FLAT" command on the disordered rings and the enhanced rigid-bond restraint was applied globally.

d) Solvent Treatment Details. The solvent masking procedure as implemented in Olex2 was used to remove the electronic contribution of solvent molecules from the refinement. As the exact solvent content is not known, only the atoms used in the refinement model are reported in the formula here. Total solvent accessible volume / cell = 626.7 Å^3 [21.0%] Total electron count / cell = 171.6

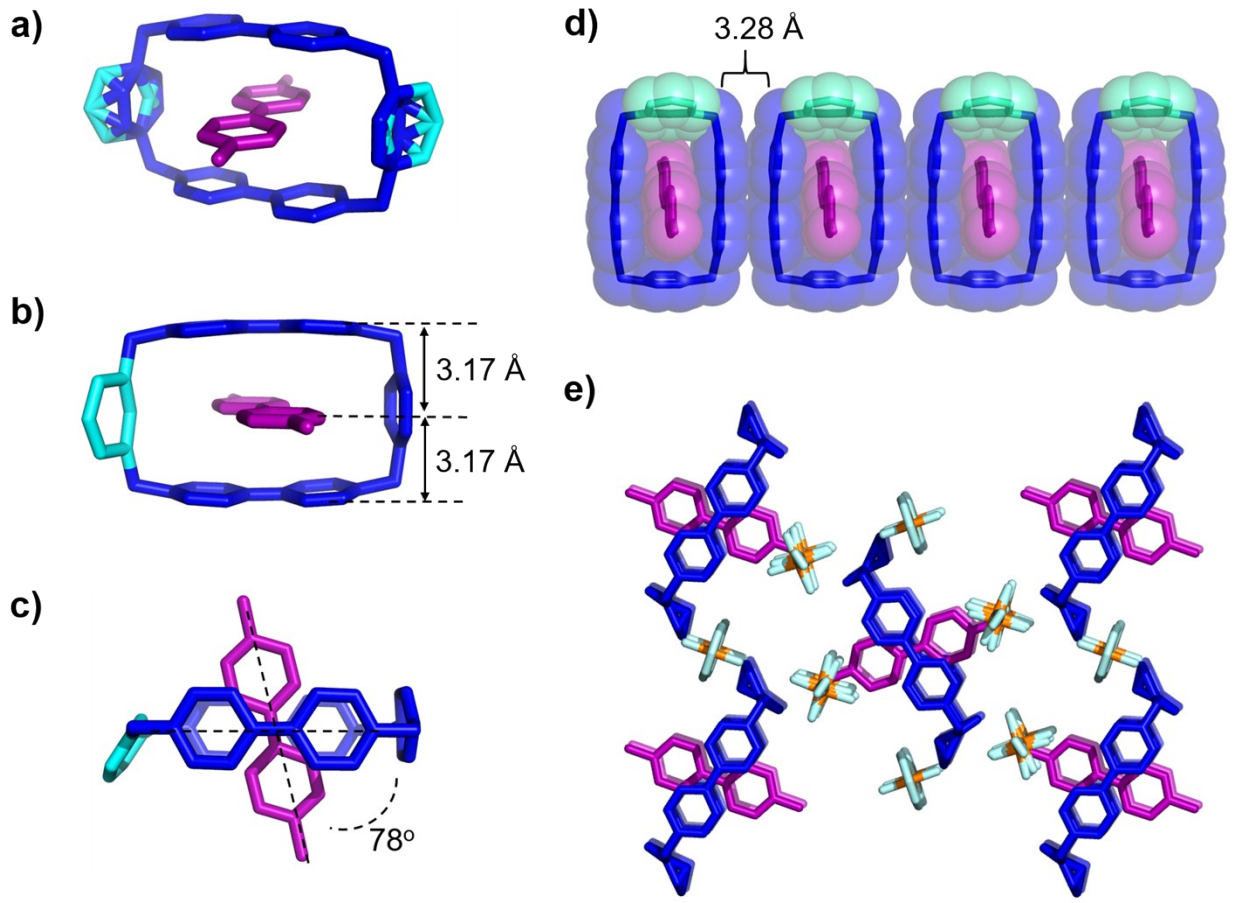

Figure S14. Solid-state (super)structure of **MV⊂mpBB**•3PF_6. a)-b) Side view, c) top view, d) 1D packing along *c*-axis. e) top view of 2D packing along c-axis. Disorder present in *p*-/*m*- xylylene moieties, which are omitted in b)-d) for the sake of clarity. Solvent molecules and counterions are omitted for the sake of clarity.

8) MV⊂PyBB•3PF_6

a) Methods. Single crystals of **MV⊂PyBB**•3PF_6 were grown in a glovebox under Ar by preparing a 2 mL solution of 1.0 mM **PyBB**•4PF_6 and 1.0 mM **MV**•2PF_6 in MeCN, followed by the addition of an excess of Zn dust. The resulting suspension was filtered and the filtrate divided between eight culture tubes. Slow vapor diffusion of $^{i}Pr_2O$ into the MeCN solutions led to the formation of purple crystals during a 5-day period.

b) Data. Orthorhombic, space group *Pbam* (no. 55), a = 14.1183(9), b = 21.8905(11), c = 9.5412(5) Å, V = 2948.8(3) Å^3, Z = 2, T = 99.98 K, $\mu(CuK_\alpha)$ = 1.768 mm^{-1}, D_{calc} = 1.287 g/mm^3, 10929 reflections measured (7.45 ≤ 2Θ ≤ 130.124), 2676 unique (R_{int} = 0.0324, R_{sigma} = 0.0289) which were used in all calculations. The final R_1 was 0.1250 ($I > 2\sigma(I)$) and wR_2 was 0.4081 (all data).

c) Refinement Details. No special refinement necessary

d) Solvent Treatment Details. The solvent masking procedure as implemented in Olex2 was used to remove the electronic contribution of solvent molecules from the refinement. As the exact solvent content is not known, only the atoms used in the refinement model are reported in the formula here. Total solvent accessible volume / cell = 690.2 Å^3 [23.4%] Total electron count / cell = 155.2

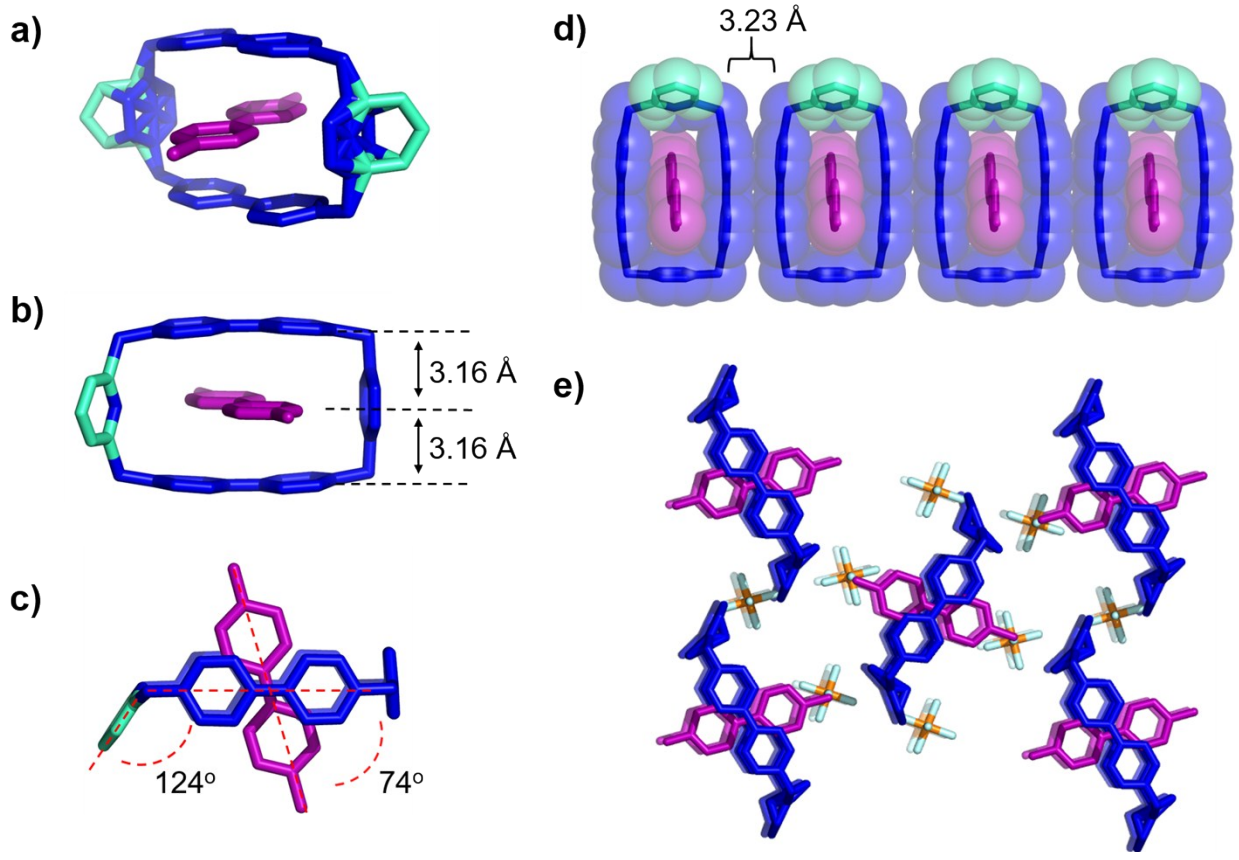

Figure S15. Solid-state (super)structure of **MV⊂PyBB**•3PF$_6$. a)-b) Side view, c) top view, d) 1D packing along *c*-axis. e) top view of 2D packing along *c*-axis. Disorder presents in benzene and pyridine moieties, which are omitted in b)-d) for the sake of clarity. Solvent molecules and counterions are omitted for the sake of clarity.

9) MV⊂DThBB•3PF$_6$

a) Methods. Single crystals of **MV⊂DThBB**•3PF_6 were grown in a glovebox under Ar by preparing a 2 mL solution of 1.0 mM **DThBB**•4PF_6 and 1.0 mM **MV**•2PF_6 in MeCN, followed by the addition of an excess of Zn dust. The resulting suspension was filtered and the filtrate divided between eight culture tubes. Slow vapor diffusion of $^{i}Pr_2O$ into the MeCN solutions led to the formation of purple single crystals during a 5-day period.

b) Data. Orthorhombic, space group *Pbam* (no. 55), a = 14.8195(8), b = 20.8662(12), c = 9.5394(7) Å, V = 2949.8(3) Å^3, Z = 2, T = 99.99 K, $\mu(CuK_\alpha)$ = 2.411 mm^{-1}, D_{calc} = 1.299 g/mm^3, 9385 reflections measured (7.316 ≤ 2Θ ≤ 127.648), 2597 unique (R_{int} = 0.0471, R_{sigma} = 0.0539) which were used in all calculations. The final R_1 was 0.1123 ($I > 2\sigma(I)$) and wR_2 was 0.3018 (all data).

c) Refinement Details. No special refinement necessary.

d) Solvent Treatment Details. The solvent masking procedure as implemented in Olex2 was used to remove the electronic contribution of solvent molecules from the refinement. As the exact solvent content is not known, only the atoms used in the refinement model are reported in the formula here. Total solvent accessible volume / cell = 812.6 Å^3 [27.5%] Total electron count / cell = 206.4

9) MV⊂ThBB•3PF$_6$

a) Methods. Single crystals of **MV⊂ThBB**•3PF_6 were grown in a glovebox under Ar by preparing a 2 mL solution of 1.0 mM **ThBB**•4PF_6 and 1.0 mM **MV**•2PF_6 in MeCN, followed by the addition of an excess of Zn dust. The resulting suspension was filtered and the filtrate divided between eight culture tubes. Slow vapor diffusion of $^{i}Pr_2O$ into the MeCN solutions led to the formation of purple single crystals during a 5-day period.

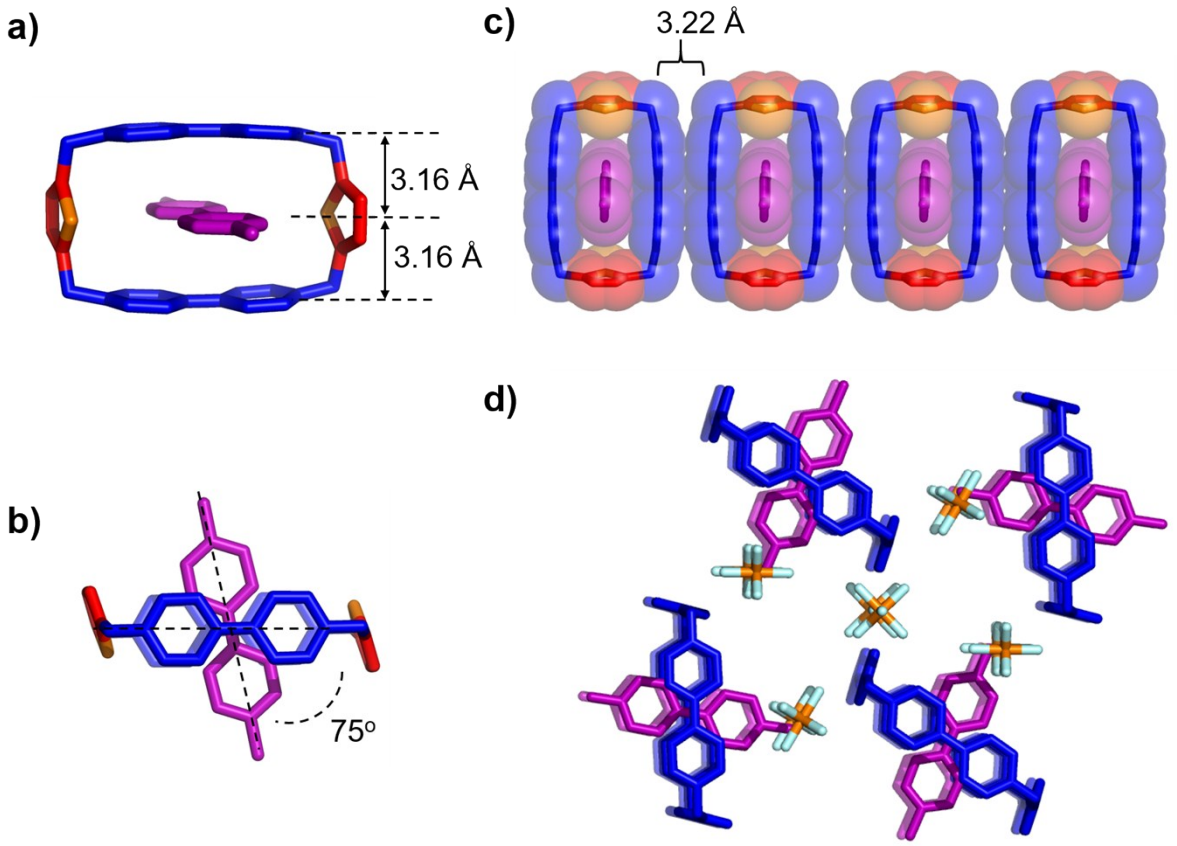

Figure S16. Solid-state (super)structure of **MV⊂DThBB**•3PF_6. a)-b) Side view, c) top view, d) 1D packing along *c*-axis. e) top view of 2D packing along c-axis. Solvent molecules and counterions are omitted for the sake of clarity.

b) Data. Orthorhombic, space group *Pbam* (no. 55), $a = 14.8597(15)$, $b = 21.003(2)$, $c = 9.5902(9)$, $V = 2993.1(5)$ Å^3, $Z = 2$, $T = 99.95$ K, $\mu(CuK_\alpha) = 2.044$ mm^{-1}, $D_{calc} = 1.245$ g/mm^3, 12833 reflections measured ($7.288 \leq 2\Theta \leq 131.324$), 2655 unique ($R_{int} = 0.0833$, $R_{sigma} = 0.0638$) which were used in all calculations. The final R_1 was 0.1358 ($I > 2\sigma(I)$) and wR_2 was 0.3577 (all data).

c) Refinement Details. Rigid bond restraints were imposed on the displacement parameters as well as restraints on similar amplitudes separated by less than 1.7 Ang globally. Distance restraints were imposed on the disordered PF_6^- anion. C9 was restrained esd (0.01) that its Uij components approximate to isotropic.

d) Solvent Treatment Details. The solvent masking procedure as implemented in Olex2 was used to remove the electronic contribution of solvent molecules from the refinement. As the exact solvent content is not known, only the atoms used in the refinement model are reported in the formula here. Total solvent accessible volume / cell = 754.1 $Å^3$ [25.6%] Total electron count / cell = 197.6

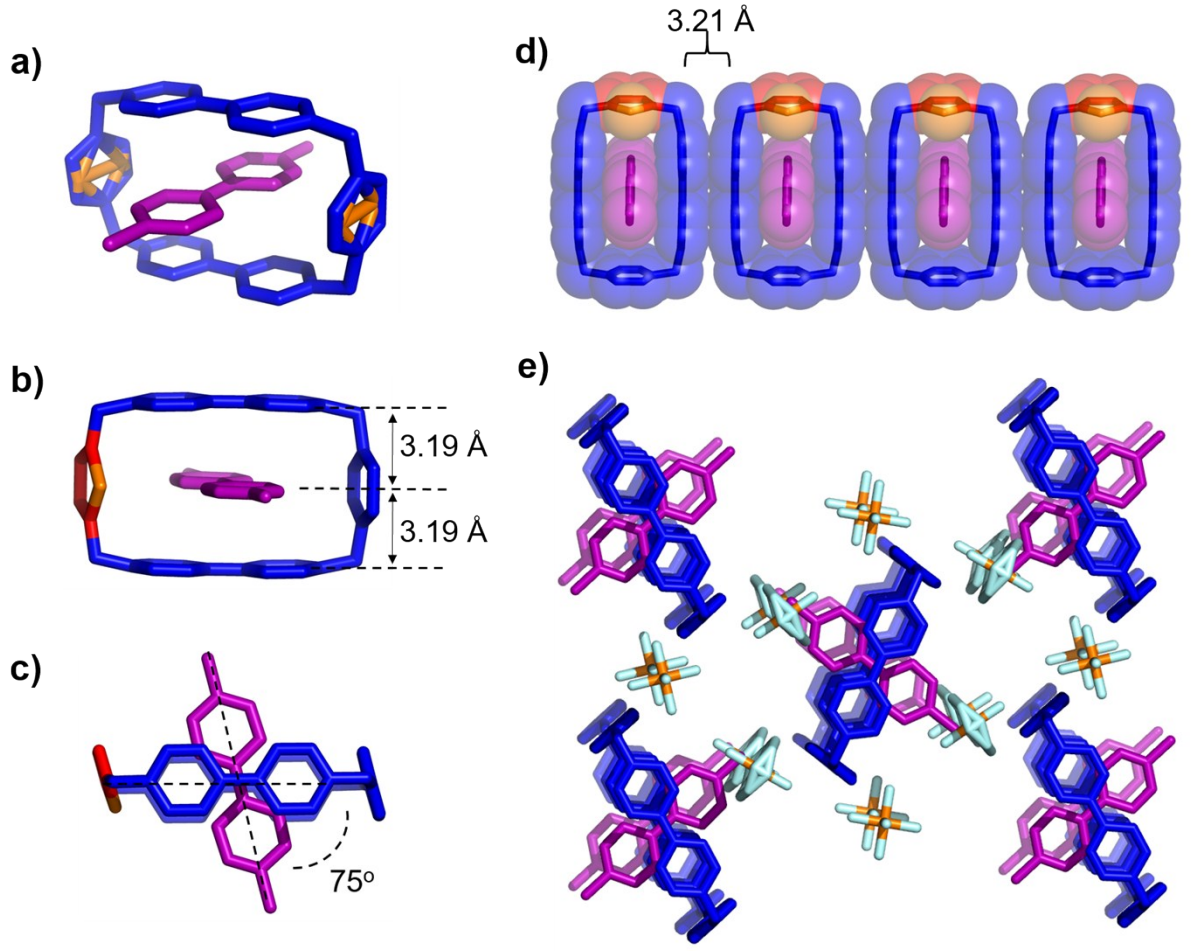

Figure S17. Solid-state (super)structure of **MV⊂ThBB**•3PF_6. a)-b) Side view; c) top view; d) 1D packing along *c*-axis; e) top view of 2D packing along c-axis. Disorder present in *p*-phenyl and thiophenyl moieties, which are omitted in b)-d) for the sake of clarity. Solvent molecules and counterions are omitted for the sake of clarity.

Section G. DFT Calculations

Geometry optimizations were performed with the PBE flavor of generalized gradient approximation as implemented in the Amsterdam Density Functional Program (ADF 2017.113)[S7]. The Slater-type orbital (STO) basis sets of double-zeta polarized quality were employed[S8]. The 1s shells of C, N and S were treated with frozen core approximation. The D3[S9] van der Waals correction with Becke-Johnson damping was included to describe the noncovalent interactions in these systems.

Single point energies were calculated based on the PBE-optimized structures with B3LYP-D3 functionals in the presence of the conductor-like screening model (COSMO) for MeCN[S10-S16]. Triple-zeta basis sets with two polarization functions (TZ2P) were applied with the same frozen core approximation as that in geometry optimizations. The ghost atom feature in ADF was employed to correct the basis set superposition error (BSSE).

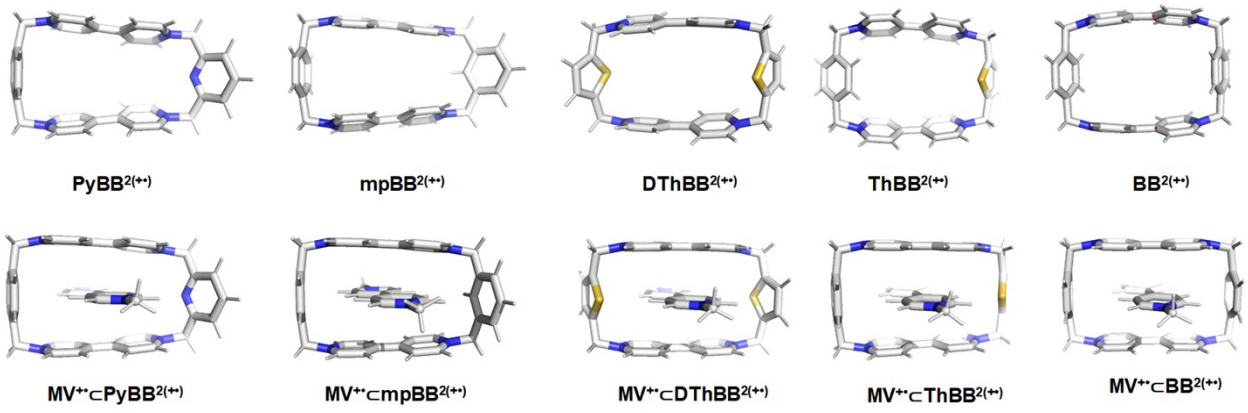

Figure S18. Optimized computational model (super)structures of diradical dicationic cyclophanes (up) and trisradical tricationic complexes (bottom)

Table S1. Comparison of the binding energies from DFT calculations and Experiments

	d/Å[a]	E_{Calc}/(kJ mol^{-1})[b]	E_{Calc_corr}/(kJ mol^{-1})[c]	E_{Exp}/(kJ mol^{-1})[d]
ThBB	6.350	-103.7	-84.0	-29.9
BB	6.705	-102.2	-82.4	-26.2
DThBB	5.975	-100.4	-80.5	-27.5
mpBB	5.725	-95.1	-74.6	-22.1
PyBB	5.495	-91.2	-70.9	-22.5

[a] the centroid-to-centroid distance (Figure 3c) between the two BIPY$^{\bullet+}$ units for the of diradical dicationic cyclophanes; [b] the binding energies with the basis set superposition error (BSSE) correction for the trisradical tricationic complexes; [c] the binding energies without the basis set superposition error (BSSE) correction for the trisradical tricationic complexes; [d] the binding energies calculated from UV-Vis-NIR titration results

Table S2. Decomposition of energies of B3LYP with no BSSE correction into dispersion and electrostatic contributions

	d/Å[a]	E_{disp}/(kJ mol^{-1})[b]	E_{sta}/(kJ mol^{-1})[c]	E_{Calc}/(kJ mol^{-1})[d]
ThBB	6.350	-191.5	87.8	-103.7
BB	6.705	-191.0	88.8	-102.2
DThBB	5.975	-197.45	97.0	-100.45
mpBB	5.725	-201.2	106.1	-95.1
PyBB	5.495	-201.6	110.4	-91.2

[a] the centroid-to-centroid distance (Figure 3c) between the two BIPY$^{\bullet+}$ units for the of diradical dicationic cyclophanes; [b] the dispersion energies without the basis set superposition error (BSSE) correction for the trisradical tricationic complexes; [c] the electrostatic repulsion energies without the basis set superposition error (BSSE) correction for the trisradical tricationic complexes; [d] the binding energies without the basis set superposition error (BSSE) correction for the trisradical tricationic complexes.

Section H. References

(S1) P. R.Ashton, J. A. Preece, J. F. Stoddart, M. S. Tolley, A. J. P. White, D. J. Williams. *Synthesis* **1994**, *12*, 1344–1352.

(S2) a) M. B. Nielsen, J. G. Hansen, J. Becher, *Eur. J. Org. Chem.* **1999**, *11*, 2807–1352.; b) H.

Scheytza, O. Rademacher, H.-U. Reißig, *Eur. J. Org. Chem.* **1999**, *9*, 2373–2381.

(S3) J. C. Barnes, M. Juríček, N. A. Vermeulen, E. J. Dale, J. F. Stoddart, *J. Org. Chem.* **2013**, *78*, 11962–11969.

(S4) M. B. Nielsen, J. G. Hansen and J. Becher, *Eur. J. Org. Chem.* **1999**, *11*, 2807–2815.

(S5) H. Scheytza, O. Rademacher and H. ‐ U. Reißig, *Eur. J. Org. Chem*. **1999**, *9*, 2373–2381.

(S6) C. Cheng, T. Cheng, H. Xiao, M. D. Krzyaniak, Y. Wang, P. R. McGonigal, M. Frasconi, J. C. Barnes, A. C. Fahrenbach, M. R. Wasielewski, W. A. Goddard, J. F. Stoddart, *J. Am. Chem. Soc.* **2016**, *138*, 8288–8300.

(S7) a) ADF2017, SCM, https://www.scm.com; b) J. P. Perdew, K. Burke, M. Ernzerhof, *Phys. Rev. Lett.* **1996,** *77*, 3865–3868.

(S8) E. V. Lenthe, E. J. Baerends, *J. Comput Chem.* **2003,** *24*, 1142–1156.

(S9) S. Grimme, S. Ehrlich, L. Goerigk, *J. Comput Chem.* **2011,** *32*, 1456–1465.

(S10) A. D. Becke, *Phys. Rev. A* **1988,** *38*, 3098–3100.

(S11) C. Lee, W. Yang, R. G. Parr, *Phy. Rev. B* **1988,** *37*, 785–789.

(S12) Y. Zhao, D. G.Truhlar, *Theor. Chem. Acc.* **2008,** *120*, 215–241.

(S13) Y. Zhao, D. G.Truhlar, *J. Chem. Phys.* **2006,** *125*, 194101.

(S14) A. Klamt, *J. Chem. Phys.* **1995,** *99*, 2224–2235.

(S15) A. Klamt, G. Schüürmann, *J. Chem. Soc. Perkin Transactions* **1993**, 5, 799–805.

(S16) A. Klamt, V. Jonas, *J. Chem. Phys.* **1996,** *105*, 9972–9981.